BIOCHEMISTRY
including biophysical chemistry & molecular biology

Article

pubs.acs.org/biochemistry

n-Alkylboronic Acid Inhibitors Reveal Determinants of Ligand Specificity in the Quorum-Quenching and Siderophore Biosynthetic Enzyme PvdQ

Kenneth D. Clevenger,[†,#] Rui Wu,[‡,#] Dali Liu,[*,‡] and Walter Fast[*,§,⊥]

[§]Medicinal Chemistry Division, College of Pharmacy, [†]Biochemistry Graduate Program, and [⊥]Center for Infectious Disease, The University of Texas, Austin, Texas 78712, United States

[‡]Department of Chemistry and Biochemistry, Loyola University Chicago, Chicago, Illinois 60660, United States

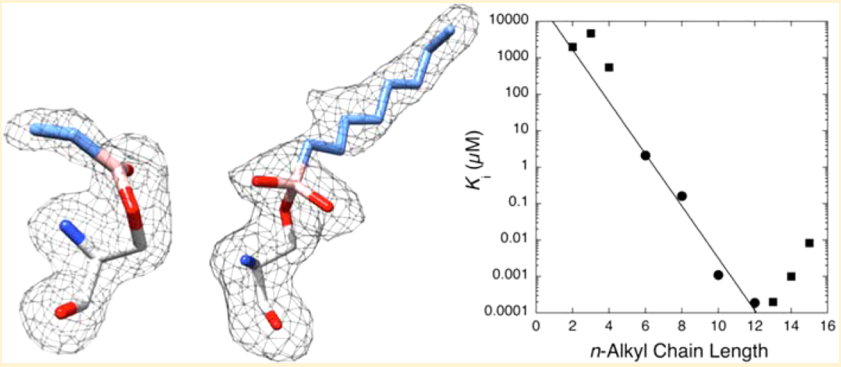

ABSTRACT: The enzyme PvdQ (E.C. 3.5.1.97) from *Pseudomonas aeruginosa* is an *N*-terminal nucleophile hydrolase that catalyzes the removal of an *N*-myristyl substituent from a biosynthetic precursor of the iron-chelating siderophore pyoverdine. Inhibitors of pyoverdine biosynthesis are potential antibiotics since iron is essential for growth and scarce in most infections. PvdQ also catalyzes hydrolytic amide bond cleavage of selected *N*-acyl-L-homoserine lactone quorum-sensing signals used by some Gram-negative pathogens to coordinate the transcription of virulence factors. The resulting quorum-quenching activity of PvdQ has potential applications in antivirulence therapies. To inform both inhibitor design and enzyme engineering efforts, a series of *n*-alkylboronic acid inhibitors of PvdQ was characterized to reveal determinants of ligand selectivity. A simple homologation series results in compounds with K_i values that span from 4.7 mM to 190 pM, with a dependence of ΔG_{bind} values on chain length of −1.0 kcal/mol/CH_2. X-ray crystal structures are determined for the PvdQ complexes with 1-ethyl-, 1-butyl-, 1-hexyl-, and 1-octylboronic acids at 1.6, 1.8, 2.0, and 2.1 Å resolution, respectively. The 1-hexyl- and 1-octylboronic acids form tetrahedral adducts with the active-site *N*-terminal Ser217 in the *β*-subunit of PvdQ, and the *n*-alkyl substituents are bound in the acyl-group binding site. The 1-ethyl- and 1-butylboronic acids also form adducts with Ser217 but instead form trigonal planar adducts and extend their *n*-alkyl substituents into an alternative binding site. These results are interpreted to propose a ligand discrimination model for PvdQ that informs the development of PvdQ-related tools and therapeutics.

The clinical need for effective drugs to combat antibiotic resistant infections has fueled interest in novel antibacterial and antivirulence strategies. In the pursuit of agents to counter *Pseudomonas aeruginosa* infections, two of these strategies, blocking siderophore biosynthesis[1] and blocking quorum-sensing,[2] intersect in the study of a hydrolytic enzyme in the *N*-terminal nucleophile hydrolase superfamily[3] called PvdQ (E.C. 3.5.1.97).[4,5] This periplasmic[6] enzyme uses an *N*-terminal Ser residue and covalent catalysis to hydrolyze an *N*-myristic (or *N*-myristoleic[7]) acid substituent from a biosynthetic precursor of the iron-scavenging siderophore pyoverdine (also spelled pyoverdin, Figure 1).[7−10] *P. aeruginosa* strains lacking a functional PvdQ do not produce pyoverdine,[5] are severely growth impaired at low iron concentrations,[11] and have reduced virulence in a *Caenorhabditis elegans* infection model.[11] Other pyoverdine-deficient strains of *P. aeruginosa* show growth inhibition in iron-deficient media,[12] in a chronic lung infection rat model,[13] in a mouse intraperitoneal infection competition assay,[13] and in a mouse infected burn model.[12] Small molecule PvdQ inhibitors have recently been developed to achieve this antibiotic effect.[9,10,14] In addition to the pyoverdine precursor substrate, PvdQ can also hydrolyze the amide bond in *N*-acyl-L-homoserine lactone quorum-sensing signals used by numerous Gram-negative bacteria.[4,10,15] Of the signals produced by *P. aeruginosa*, *N*-butanoyl-L-homoserine lactone is not hydrolyzed by PvdQ,[4] and *N*-3-oxo-dodecanoyl-L-homoserine lactone appears to be a disfavored substrate due to its 3-oxo substituent (Figure 1).[10] Nevertheless, PvdQ

Received: August 28, 2014
Revised: October 6, 2014
Published: October 7, 2014

   dx.doi.org/10.1021/bi501086s | *Biochemistry* 2014, 53, 6679−6686

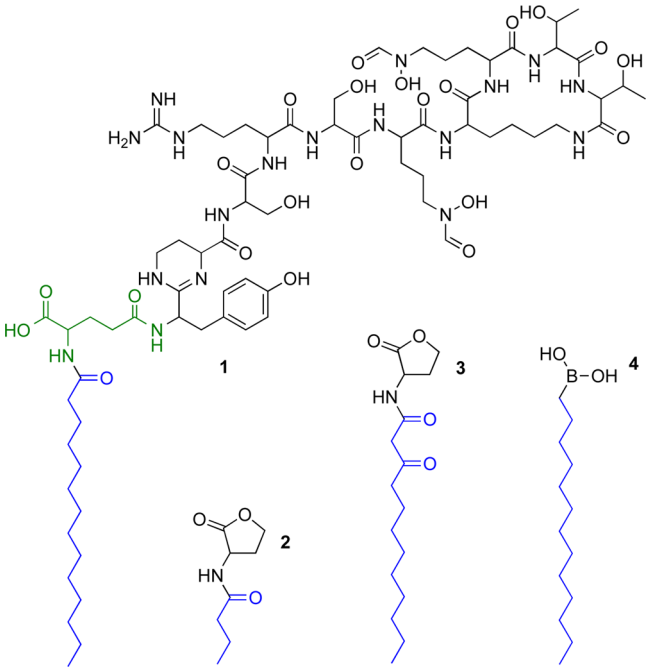

Figure 1. Selected PvdQ ligands and related compounds. The common *n*-alkyl substituent is colored in blue and the differing "head groups" are in black for the *N*-myristylated pyoverdine precursor[7] (**1**, with the glutamine residue linker in green), the *P. aeruginosa* quorum-sensing signals *N*-butanoyl-L-homoserine lactone (**2**) and *N*-3-oxo-dodecanoyl-L-homoserine lactone (**3**), and the transition state analogue 1-tridecylboronic acid (**4**). An alternate version of the *N*-myristylated pyoverdine precursor has also been proposed in which cyclization of the quinolone chromophore of mature pyoverdine has already taken place.[9]

overepxression is sufficient to inhibit *P. aeruginosa* quorum sensing and reduce virulence in a *C. elegans* infection model,[15] and formulations of the purified protein have been developed to facilitate inhalational therapies.[16] Recent efforts have also re-engineered PvdQ to improve hydrolysis of the substrate *N*-octanoyl-L-homoserine lactone and effectively applied this variant enzyme as an antivirulence agent in a moth larvae model of *Burkholderia* infection.[17] Therefore, the development of more effective PvdQ variants as therapeutic enzymes is also of interest.

However, both the design of small molecule PvdQ inhibitors and the engineering of PvdQ selectivity are hampered, in part, by two unresolved aspects of ligand recognition. First, the mechanism of substrate discrimination has not been fully determined. Previously, a hydrophobic "acyl-group" binding site in PvdQ was identified through X-ray crystallography and probed by site-directed mutagenesis.[8−10,17] By steric occlusion, the limited size and shape of this cavity likely disfavor the binding and processing of substrates too large to be accommodated. For example, comparison of structural models and steady-state kinetic analysis suggests that a narrowing of the acyl-group binding site near P238 and the backbone of H284 disfavors processing of *N*-3-oxo-dodecanoyl-L-homoserine lactone approximately 100-fold[10] over unsubstituted substrates. However, since steric occlusion of smaller compounds is not a likely mechanism, it is unclear how PvdQ excludes potential substrates with *n*-acyl substituents containing ≤8 carbons, such as *N*-butanoyl-L-homoserine lactone.[4,10] Second, inhibitors that target the "head-group" binding site found in PvdQ have not been reported. This headgroup binding site is much larger and more functionally diverse than the acyl-group binding site and is expected to accommodate the diverse leaving groups of various substrates, including the large cyclic peptide of the pyoverdine precursor. Potent PvdQ inhibitors derived from high-throughput screening all bind deep within the hydrophobic acyl-group binding site and, with the exception of ≤2 H-bond(s) each, appear to derive their binding energy through hydrophobic interactions.[9,14] Specific H-bonding often drives inhibitor selectivity[18] and contributes to the enthalpic component of binding favored in drug lead identification,[19] so targeting the more polar headgroup binding site is desirable. However, apart from the reversible covalent S217−O^{γ}-boron bond formed by *n*-alkylboronic acids (Figure 1),[10] PvdQ inhibitors that instead target the catalytic residues or the more polar headgroup binding site are not known.

Although fatty acids and substrates with *n*-alkyl substituents ≤8 carbons are not well bound or processed by PvdQ,[4,10] we reasoned that the enhanced affinity of *n*-alkylboronic acids, which are approximately 5000-fold more potent than structurally similar fatty acids,[10] might enable us to characterize the interaction of PvdQ with ligands bearing shorter *n*-alkyl chains. Characterization of the binding of smaller ligands may help to elucidate how *N*-butanoyl-L-homoserine lactone and other structurally related signals avoid PvdQ processing. So, to better define the mechanism of PvdQ substrate discrimination and to reveal determinants of ligand recognition and discrimination, we report here the affinity and structural characterization of a series of *n*-alkylboronic acid inhibitors.

MATERIALS AND METHODS

Materials. Unless otherwise noted, all chemicals were from Sigma-Aldrich Chemical Co. (St. Louis, MO, USA). 1-Ethylboronic acid (C2-$B(OH)_2$), 1-propylboronic acid (C3-$B(OH)_2$), 1-butylboronic acid (C4-$B(OH)_2$), 1-hexylboronic acid (C6-$B(OH)_2$), and 1-octylboronic acid (C8-$B(OH)_2$) were from Alfa Aesar (Ward Hill, MA, USA). Boronic acids with longer *n*-alkyl substituents were obtained and abbreviated as described previously.[10] Graphing and curve fitting was performed using KaleidaGraph 3.6 (Synergy Software, Reading, PA, USA).

Expression and Purification of PvdQ. Recombinant *P. aeruginosa* PvdQ containing a C-terminal His_6-affinity tag was expressed and purified in Tuner (DE3) pLysS *Escherichia coli* cells (EMD Millipore) and stored in 10% (v/v) glycerol at −80 °C as described previously.[10]

Determining *n*-Alkylboronic Acid K_i Values. Determination of potency for C2-, C3-, C4-, and C6-$B(OH)_2$ inhibition of purified PvdQ was accomplished using procedures similar to those described previously.[10] Briefly, stock solutions of the colorimetric PvdQ substrate (4-nitrophenyl dodecanoate)[9,10] were prepared in methanol and stock solutions of each *n*-alkylboronic acid inhibitor in DMSO. Continuous spectrophotometric kinetic assays were used to determine initial hydrolysis rates by mixing substrate (5 μM), and *n*-alkylboronic acid inhibitor (ranging from 0.002−60 mM depending on the compound, typically with three concentrations above and below each IC_{50} value) in Na_2HPO_4 buffer (40 mM) at pH 8.0 and 25 °C, each reaction being made to a final 20% methanol cosolvent[10] concentration in a disposable 1 mL polystyrene cuvette (Thermo Fisher). Each reaction was initiated by addition of purified PvdQ (10 nM) and product formation was monitored by measuring the increase in absorbance at 402 nm

dx.doi.org/10.1021/bi501086s | *Biochemistry* 2014, 53, 6679−6686

continuously, using an ε_{402nm} = 13 000 M^{-1} cm^{-1} that was determined experimentally using assay buffer and a *p*-nitrophenol standard. As a benchmark for solubility of the more hydrophobic compounds tested, we considered the critical micelle concentration values of the structurally related compounds *N*-dodecanoyl-L-homoserine lactone (4 μM), *N*-3-oxo-dodecanoyl-L-homoserine lactone (247 μM), and the ring-opened compound *N*-dodecanoyl-L-homoserine (>400 μM),[20] which were all significantly higher than the concentrations used here for ligands of similar length, even without considering the effects of methanol cosolvent, which is known to significantly increase the critical micelle concentration value of a common detergent.[21] Plots of *n*-alkyboronic acid concentration versus percent inhibition were fitted to the equation: % inhibition = $(100/(1 + (IC_{50}/[I])^h))$, where [I] stands for the concentration of *n*-alkylboronic acid and *h* for the Hill coefficient. The Hill coefficient was kept variable as a diagnostic method to flag compounds that might cause inhibition by inducing protein denaturation or inhibit as their micellular forms ($h \gg 1$), or to flag compounds that might aggregate or become insoluble at higher concentrations ($h \ll 1$).[22] The Hill coefficients for this compound series were all determined by fitting to be within the 0.7−0.9 range and so were not flagged as inhibitors with problematic inhibition mechanisms. Using a competitive inhibition model, IC_{50} values were converted into K_i values using the equation:[23] $IC_{50} = K_i(1 + ([S]/K_M))$, where [S] is the substrate concentration (5 μM), and K_M = 0.8 μM.[10] Compounds C2-, C3-, C4-, and C6-B$(OH)_2$ were not tight-binding inhibitors and so did not require the analysis described previously for the longer-chained more-potent *n*-alkylboronic acids.[10] The ΔG_{bind} values were calculated for each compound using the equation: $\Delta G = -RT \ln(1/K_i)$, where R = 1.98 cal/Kmol and T = 298 K. Propagated errors are derived from the initial fitting errors for IC_{50} values.

Crystallization, Crystal Soaking, and Data Collection. Crystals of purified PvdQ were grown via hanging drop vapor diffusion by mixing 1 μL of PvdQ (10 mg/mL) with 1 μL of reservoir solution (Hepes (50 mM) at pH 7.5; RbCl (80 mM); PEG-4000 (10% (w/v)). Crystals were grown at ambient temperature (approximately 25 °C) and displayed good morphology within 5 days. Diffraction quality crystals were soaked in reservoir solution supplemented with *n*-alkylboronic acid inhibitors (10 mM of C2-, C4-, C6-B$(OH)_2$, or 20 μM of C8-B$(OH)_2$), methanol (50% v/v) and glycerol (20% v/v) as cryoprotectant before flash freezing in liquid nitrogen. Crystallographic data were collected on beamline 23-ID-B and 23-ID-D of GM/CA-CAT at the Advance Photon Source (APS) using X-rays of 1.054 Å wavelength and a Rayonix (formerly MAR-USA) 4 × 4 tiled charge coupled device (CCD) detector. All data were indexed, integrated, and scaled with software suite HKL2000.[24]

Phasing, Model Building, and Refinements. Rigid body refinement was used directly for phasing by starting with our previous model (protein data bank (PDB) accession code 4M1J)[10] after water molecules and the bound inhibitor (C13-B$(OH)_2$) were deleted from the coordinates. Refinement of the protein/inhibitor complex structures were carried out by restrained refinement using Refmac5[25] and further manual model inspection and adjustment using *Coot*.[26] After refinements converged, solvent molecules (water and glycerol) were added in several rounds. Ligand coordinates were not included in each refinement until the very last cycles. The F_o-F_c difference maps, before incorporation of ligands in the structures, of all four complexes showed well-defined electron density for the corresponding ligands. The inhibitors' structures were created in ChemDraw (PerkinElmer), and the program JLigand[27] was used to regularize the molecules and to generate chemical restraints. Inhibitors were fit into the residual electron density using *Coot*.[26] Further refinements were carried out using Refmac5 and PHENIX.refine.[28] The *R* factor and R_{free} for PvdQ soaked with C2-, C4-, C6- and C8-B$(OH)_2$ were 15.9/19.0, 16.5/19.2, 18.2/21.5, and 15.1/19.3, respectively. Structural analysis and comparison, including RMSD calculations and figure preparation, were completed using UCSF Chimera.[29]

RESULTS AND DISCUSSION

To better elucidate ligand interactions with PvdQ, we determined the K_i values for a series of boronic acids bearing *n*-alkyl substituents 2−15 carbons in length (Table 1 and Figure

Table 1. K_i and ΔG_{bind} Values for *n*-Alkylboronic Acid Inhibition of PvdQ

inhibitor	K_i (M)	ΔG_{bind} (kcal/mol)
C2-B$(OH)_2$	$(2.0 \pm 0.4) \times 10^{-3}$	−3.7 ± 0.2
C3-B$(OH)_2$	$(4.7 \pm 0.8) \times 10^{-3}$	−3.1 ± 0.2
C4-B$(OH)_2$	$(5.5 \pm 0.9) \times 10^{-4}$	−4.4 ± 0.2
C6-B$(OH)_2$	$(2.1 \pm 0.4) \times 10^{-6}$	−7.7 ± 0.2
C8-B$(OH)_2$[a]	$(1.61 \pm 0.03) \times 10^{-7}$	−9.23 ± 0.02
C10-B$(OH)_2$[a]	$(1.1 \pm 0.4) \times 10^{-9}$	−12.2 ± 0.4
C12-B$(OH)_2$[a]	$(1.9 \pm 0.2) \times 10^{-10}$	−13.2 ± 0.1
C13-B$(OH)_2$[a]	$(2.0 \pm 0.4) \times 10^{-10}$	−13.2 ± 0.2
C14-B$(OH)_2$[a]	$(1.0 \pm 0.3) \times 10^{-9}$	−12.2 ± 0.3
C15-B$(OH)_2$[a]	$(8.3 \pm 0.9) \times 10^{-9}$	−11.0 ± 0.1

[a]Values taken from Clevenger et al.[10]

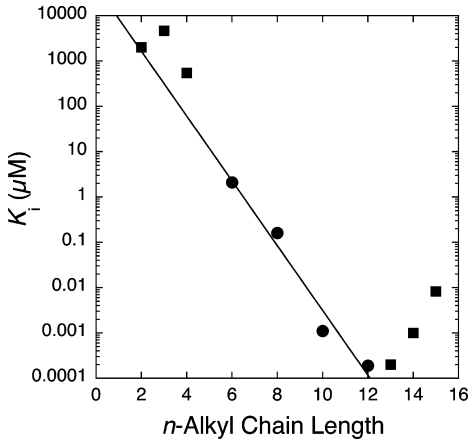

Figure 2. K_i value variation with *n*-alkyl chain length. Inhibition constants for a series of *n*-alkylboronic acids vary from mM to pM values, depending on *n*-alkyl chain length. An exponential fit to the K_i values (log scale) for C6-, C8-, C10-, and C12-B$(OH)_2$ inhibitors (●) is shown, while the shorter and longer inhibitors (■) are excluded from fitting (see Results and Discussion). A corresponding linear fit to the ΔG_{bind} values for these four inhibitors (not shown) gives a slope of −1.0 ± 0.1 kcal/mol/CH_2, showing the average change in binding energy as the *n*-alkyl chain length varies, and an intercept of −1.8 ± 1 kcal/mol, predicting the binding energy of boric acid (an *n*-alkyl chain length of zero).

dx.doi.org/10.1021/bi501086s | *Biochemistry* 2014, 53, 6679−6686

Table 2. Crystallographic Data for PvdQ/Inhibitor Complexes

	PvdQ:C2-B(OH)$_2$	PvdQ:C4-B(OH)$_2$	PvdQ:C6-B(OH)$_2$	PvdQ:C8-B(OH)$_2$
Data Processing				
space group	$C222_1$	$C222_1$	$C222_1$	$C222_1$
cell dimension				
α, β, γ (deg)	121.9; 167.5; 94.5	121.3; 167.5; 95.0	121.1; 168.2; 94.9	120.7; 166.5; 94.5
a, b, c (Å)	90; 90; 90	90; 90; 90	90; 90; 90	90; 90; 90
resolution (Å)	42.6−1.6	47.5−1.8	39.0−2.0	47.3−2.1
R_{merge} (%)[a]	7.8 (83.4)[b]	15.9 (100)[b]	24.1 (100)[b]	13.4 (81.3)[b]
$I/\sigma(I)$	12.7 (1.4)	10.1 (1.2)	5.4(1.6)	13.1(3.1)
completeness (%)	99.5(100)	99.9(100)	99.2(98.7)	99.9(99.7)
multiplicity	3.8 (3.7)	5.7 (5.8)	5.1 (5.1)	7.5 (7.6)
no. reflections	453318	527445	327941	393018
no. unique reflections	119528	92191	64713	52338
Refinement				
R_{work}[c]/R_{free}[d] (%)	15.9/19.0	16.5/19.2	18.2/21.5	15.1/19.3
no. of atoms	6372	6361	6216	6175
protein	5587	5743	5572	4661
water	781	650	548	499
B-factors				
average	29.2	34.7	38.2	31.8
ligand (n-alkyl-B(OH)$_2$)	29.7−43.6	17.4−51.9	27.5−83.2	15.1−39.6
RMSD[e]				
bond length (Å)	0.019	0.013	0.003	0.008
bond angle (deg)	1.707	1.396	0.750	1.03
Ramachandran Statistics				
most favored (%)	97.4	97.3	95.8	96.5
allowed (%)	2.6	2.7	3.9	3.4
outliers (%)	0.00	0.00	0.3	0.1

[a] $R_{merge} = \Sigma|I_{obs} - I_{avg}|/\Sigma I_{avg}$. [b] The values for the highest resolution bin are in parentheses. [c] $R_{work} = \Sigma|F_{obs} - F_{calc}|/\Sigma F_{obs}$. [d] Five percent of the reflection data were selected at random as a test set and only these data were used to calculate R_{free}. [e] RMSD, root-mean-square deviation.

2). The affinities vary over a wide scope, with K_i values ranging from 4.7 mM (C3-B(OH)$_2$) to 190 pM (C12-B(OH)$_2$), an impressive span of 8 orders of magnitude for a simple homologation series. In general, affinity increases with chain length, although n-alkylboronic acids with substituents ≥13 carbons in length fall off this trend. This deviation likely reflects steric occlusion of the inhibitors due to the limited size of the acyl-group binding pocket in PvdQ. The C13-B(OH)$_2$ inhibitor is structurally homologous to the myristic acid substituent of the pyoverdine precursor substrate[7] and indicates that PvdQ appears to have been evolutionarily optimized for efficient catalysis of substrates containing this length n-alkyl substituent.

Binding affinity increases exponentially with n-alkyl chain length, and a corresponding plot of ΔG_{bind} values shows a linear dependence from C6- through C12-B(OH)$_2$ compounds (Figure 2). Excluding longer compounds, which are likely sterically occluded, and shorter compounds, which bind in a different conformation (vide infra), inhibitor affinity increases by −1.0 ± 0.1 kcal/mol/CH$_2$. Extrapolation to a chain length of zero estimates a K_i for borate of ∼50 mM (Figure 2). To put these values in context, the dependence of binding energy on chain length reveals a more favorable value than that measured for partitioning of small molecules between water and n-octanol (−0.68 kcal/mol/CH$_2$),[30,31] approaches the contribution of buried hydrophobic residues to protein stability (−1.3 kcal/mol/CH$_2$),[32] and falls short of the predicted maximum affinity of ligands to proteins (−1.5 kcal/mol/atom,[33] although this limit can be exceeded in particular cases[34]). Thorpe and co-workers reported a similar analysis for binding a series of n-alkyl-S-coenzyme A derivatives to medium-chain acyl-CoA dehydrogenase and found a similar exponential dependence of K_d on chain length that spans 5 orders of magnitude, but with a weaker dependence of −0.39 kcal/mol/CH$_2$.[35] Therefore, this portion of the PvdQ acyl-group binding pocket appears to be highly optimized for hydrophobic binding of n-acyl substituents.

To investigate the conformations of different sized ligands bound to PvdQ, we determined the crystal structures of PvdQ in complex with the C8-, C6-, C4- and C2-B(OH)$_2$ inhibitors, at 1.6−2.1 Å resolutions. Data collection and processing statistics are given in Table 2. Protein residues in the resulting heterodimer are numbered consecutively, as described previously,[10] with the N-terminal Ser in the β-chain assigned as Ser217. The resulting structural models of the PvdQ:C8-B(OH)$_2$ and PvdQ:C6-B(OH)$_2$ complexes were very similar overall to the previous structure we reported for the PvdQ:C13-B(OH)$_2$ complex,[10] each showing an RMSD of approximately 0.2 Å and revealing that the N-terminal S217 residues all adopt nearly identical conformations. Both models are consistent with the formation of a new dative covalent bond between the active-site S217−O$^\gamma$ and the boron of the inhibitor (Figure 3A,B,E), resulting in an anionic tetrahedral adduct that mimics the second proposed tetrahedral transition state in substrate turnover, as was observed earlier with C13-B(OH)$_2$.[10] On the basis of the simulated annealing omit density maps (F_o−F_c) shown, the n-alkyl substituent of C8-B(OH)$_2$ is more stable than that of C6-B(OH)$_2$ and corresponds with the higher affinity of this compound. The n-alkyl substituents of these

dx.doi.org/10.1021/bi501086s | Biochemistry 2014, 53, 6679−6686

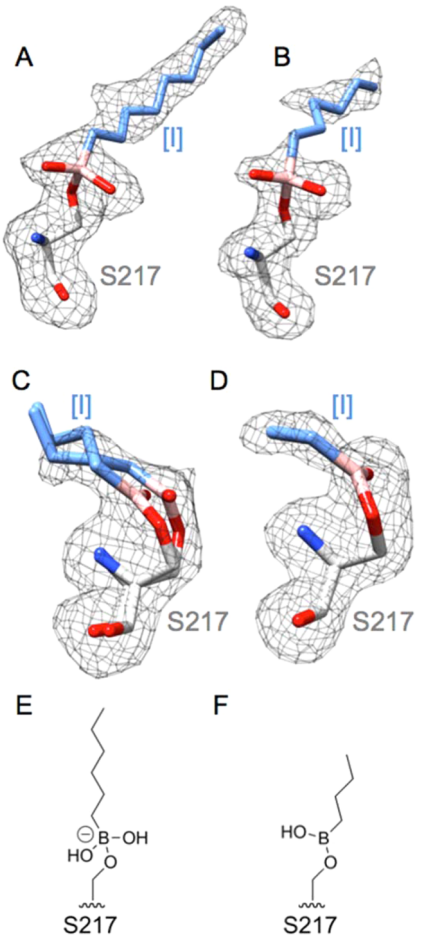

Figure 3. Ligand interpretation at the active site. The simulated annealing omit difference maps ($F_o - F_c$) are shown for PvdQ/inhibitor complexes as a gray mesh at either 2.5 σ (A, PvdQ:C8-$B(OH)_2$; B, PvdQ:C6-$B(OH)_2$ and C, PvdQ:C4-$B(OH)_2$) or 2.8 σ (D, PvdQ:C2-$B(OH)_2$). Continuous density is observed between the side chain of S217 and each inhibitor. A tetrahedral adduct is observed in the PvdQ:C8-$B(OH)_2$ (A) and PvdQ:C6-$B(OH)_2$ (B) complexes; therefore, the adducts are built with sp^3 hybridization. In contrast, the omit map densities for the PvdQ:C4-$B(OH)_2$ (C) and PvdQ:C2-$B(OH)_2$ (D) complexes are not tetrahedral but are planar in shape. So these adducts are built with sp^2 hybridization, along with a dual conformation for the *n*-alkyl substituent of the PvdQ:C4-$B(OH)_2$ adduct. (E) Line drawing of the tetrahedral adduct formed by C6-$B(OH)_2$. (F) Line drawing of the trigonal planar adduct formed by C4-$B(OH)_2$.

inhibitors each extend into the acyl-group binding pocket, albeit to different depths (Figure 4A,B).

In contrast, the structural determinations of the PvdQ:C4-$B(OH)_2$ and PvdQ:C2-$B(OH)_2$ complexes revealed significant differences in ligand binding conformation. While there are no large-scale changes in the overall protein structure (RMSD values $\leq$ 0.25 Å in comparison to the PvdQ:C13-$B(OH)_2$ structure[10]), the simulated annealing omit difference maps ($F_o - F_c$) obtained by omitting the ligand and the β-chain *N*-terminal S217 revealed extra electron density at the active site that was not well fit by a tetrahedral adduct between the inhibitor boron and the S217–O^{γ}. In comparison with the densities observed for the PvdQ:C8-$B(OH)_2$ and PvdQ:C6-$B(OH)_2$ complexes, those for the PvdQ:C4-$B(OH)_2$ and PvdQ:C2-$B(OH)_2$ complexes are more planar in nature and are better fit by modeling a trigonal planar adduct between the

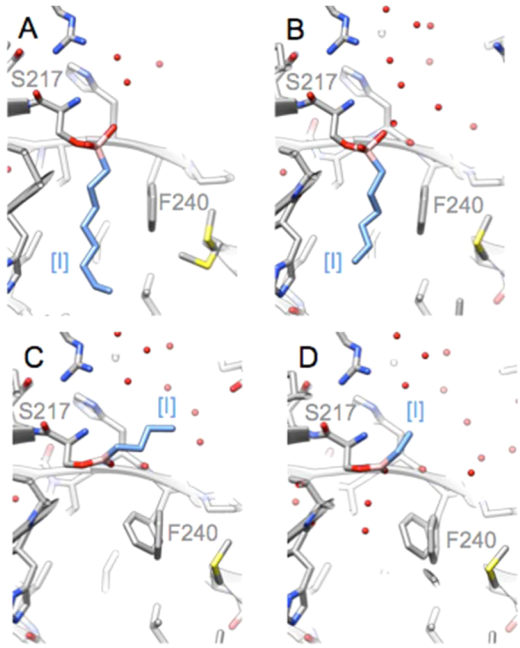

Figure 4. Differing positions of inhibitors. The structural models of the PvdQ:C8-$B(OH)_2$ complex (A) and the PvdQ:C6-$B(OH)_2$ complex (B) show an inhibitor conformation similar to that observed previously[10] with the transition-state inhibitor C13-$B(OH)_2$ by making a covalent tetrahedral adduct with the *N*-terminal S217 of the β-chain and placing their *n*-alkyl substituent in the acyl-group binding pocket. The structural models of the PvdQ:C4-$B(OH)_2$ complex (C, only one conformation of the *n*-alkyl substituent is shown for clarity) and the PvdQ:C2-$B(OH)_2$ complex (D) show an alternative inhibitor conformation in which a trigonal planar adduct is formed with S217 and the *n*-alkyl substituents are oriented instead toward the solvent-filled headgroup binding pocket. In the unfilled acyl-group binding pocket, the F240 "gate" residue now has two conformations, and the PvdQ:C2-$B(OH)_2$ complex has two ordered waters in the acyl-group binding pocket. The carbon atoms of inhibitors ([I]) are shown in blue, and protein carbon atoms are in gray, with boron in pink, oxygen in red, sulfur in yellow, and nitrogen in blue. Ordered water molecules are shown as red spheres.

Ser217-O^{γ} and the boron of these shorter chained inhibitors (Figure 3C,D,F). Therefore, the structural models are consistent with proposing instead that a neutral trivalent boron is present in the covalent adducts formed by C2- and C4-$B(OH)_2$. Boronic acids interconvert readily between these two forms (e.g., the ionization equilibrium occurs between neutral trigonal form and the anionic tetrahedral form upon hydroxide attack).[36] Although the adducts are of a different nature and the positions of the *N*-terminal S217 side chains are somewhat different, the *N*-terminal S217 amine is entirely superimposable in all of these structures. In the PvdQ:C4-$B(OH)_2$ model, one conformation of the entire S217 residue is superimposable with that of PvdQ:C13-$B(OH)_2$, but the alternative conformation has a C^{α}–C^{β} bond rotation of approximately 50°. The S217 C^{α}–C^{β} bond in the PvdQ:C2-$B(OH)_2$ complex matches this rotated configuration.

In addition to the differences in boron valence, the *n*-alkyl substituents of these shorter inhibitors are found in a different position. Instead of residing in the acyl-chain binding pocket, as with all previous PvdQ inhibitors,[9,10,14] the extra electron density in the omit maps resides outside of this pocket. The *n*-alkyl substituents fit into this density now point "outward" toward the more polar headgroup binding pocket (Figure

dx.doi.org/10.1021/bi501086s | *Biochemistry* 2014, 53, 6679–6686

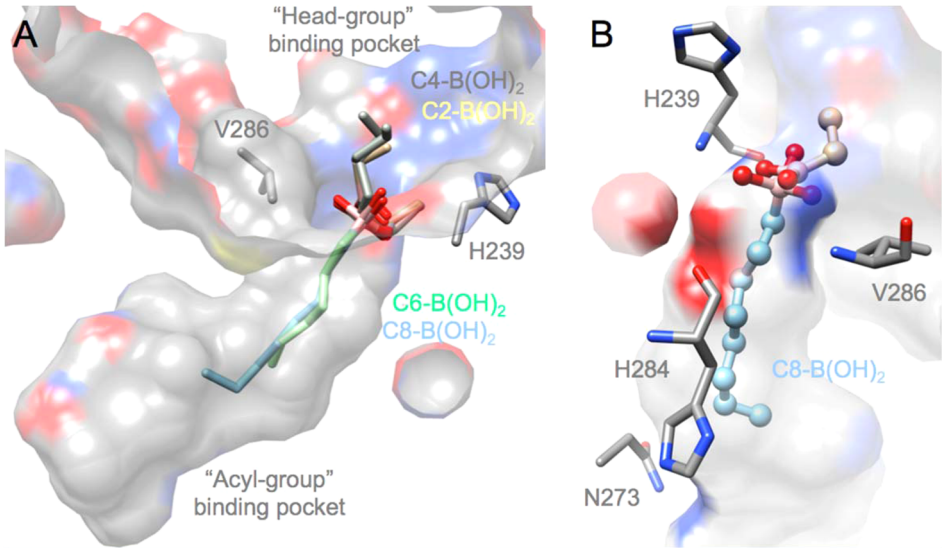

Figure 5. Binding site surfaces. (A) C2-, C4-, C6- and C8-B(OH)$_2$ inhibitors are shown in stick form relative to a surface representation of PvdQ highlighting the hydrophobic acyl-group binding site and the wider, more polar headgroup binding site. The surface is colored according to heteroatom (red for oxygen, blue for nitrogen, yellow for sulfur, pink for boron, gray for carbon). The *n*-alkyl substituents of C2- and C4-B(OH)$_2$ are oriented toward the headgroup binding site and appear to be partially stabilized through hydrophobic interactions with the side chain of V386 and the C$^{\beta}$ of H239. (B) An alternative view of the acyl-group binding site, here in complex with C2-B(OH)$_2$ (tan) and C8-B(OH)$_2$ (light blue) (both in ball and stick models), shows the backbone N of V286 and the backbone oxygens of H239 and H284 lining the start of the acyl-group binding site, resulting in a more polar entryway than is found in the rest of the site.

4C,D). Hydrophobic interactions between the first two carbons in these *n*-alkyl substituents with the C$^{\beta}$ of H239 and the side chain of V286 appear to contribute to the stabilization of this different conformation. The *n*-alkyl chain is not well stabilized after that point and likely adopts multiple conformations, accounting for the observed decrease in electron density for this part of the inhibitor in the omit map for C4-B(OH)$_2$. Along with the repositioning of the *n*-alkyl chain in both the C2- and C4-B(OH)$_2$:PvdQ complex structures, dual conformers are now observed for F240, a residue previously suggested to serve as a sort of "gate"[8] at the entryway of the acyl-group binding site to exclude solvent from the unoccupied site and is observed here approximating both the "open" and "closed" states (Figure 4C,D).

This characterization of inhibitor binding helps to reveal how PvdQ favors binding to ligands with longer *n*-alkyl substituents and discriminates against ligands with shorter substituents. For each demonstrated substrate of purified PvdQ (*N*-myrstylated pyoverdine precursor,[9] *N*-acyl-L-homoserine lactones,[4,8,10] or *n*-alkyl-*p*-nitrophenol esters[9,10]), the bulky size of each leaving group and the limited space of the acyl-group binding pocket limit how deeply *n*-alkyl substituents can bind. Substrates and inhibitors with shorter *n*-alkyl substituents can only shallowly access the entryway of the acyl-group binding pocket, which is more polar than deeper portions of the pocket, so binding is not favorable (Figure 5). For example, the *N*-butanoyl-L-homoserine lactone signal, endogenous to *P. aeruginosa*, has an *n*-alkyl substituent equivalent in length to the C3-B(OH)$_2$ inhibitor and would not be well stabilized in this polar entryway. However, in the present work, the increased affinity due to the boronic acid substituent allows us to visualize bound ligands of this smaller size and show they are instead oriented outward, toward the proposed headgroup binding site. In the structures with bound ligands bearing shorter *n*-alkyl substituents, the entryway to the acyl-group binding site is occluded by the "closed" dual conformation of the F240 "gate" residue. In the case of one complex structure, two ordered water molecules are also found in the entryway (Figure 4C,D). However, ligands with longer *n*-alkyl substituents can access a deeper portion of the acyl-group binding pocket, for which hydrophobic binding of *n*-alkyl substituents has been highly optimized, with ligand affinity increasing by −1.0 kcal/mol/CH$_2$ as the ligand enters the site, until the steric limit of the pocket is reached, with the optimal length corresponding to that near a myristic acid substituent (Figures 2 and 5). For example, the *N*-3-oxo-dodecanoyl-L-homoserine lactone signal produced by *P. aeruginosa* has an *n*-alkyl substituent equivalent in length to the C11-B(OH)$_2$ inhibitor and has sufficient length to bind to and be stabilized by the more hydrophobic part of the pathway unreachable by the smaller *N*-butanoyl-L-homoserine lactone signal. With *n*-alkylboronic acid inhibitors, the tipping point between inward and outward facing conformations occurs between C4- and C6-B(OH)$_2$ and corresponds to a ∼260-fold difference in K_i values. With substrates, k_{cat}/K_M values increase approximately 100-fold when substituents increase from C10- to C12-alkyl chains,[10] suggesting a more demanding threshold for catalysis. Although not proven here, we note the possibility that interactions with longer *n*-alkyl chains may also aid in stabilization of a reaction transition state, because these complexes are stabilized as anionic tetrahedral adducts rather than as the neutral trigonal adducts observed for shorter ligands, for which the corresponding *N*-acyl-L-homoserine lactones and *p*-nitrophenol esters are not substrates.[4,10]

There are similarities and differences of this discrimination mechanism and that proposed for the thioesterase domain in human fatty acid synthase, an enzyme that also enforces selectivity for acyl chains of a defined length. Thioesterase appears to tether the hydrophobic terminus of the *n*-acyl substituent of a substrate into a closed pocket, with the rest of the hydrophobic chain binding along an exposed groove.[37,38] As with PvdQ, substrates with *n*-acyl substituents longer than

dx.doi.org/10.1021/bi501086s | *Biochemistry* 2014, 53, 6679−6686

desired appear to be sterically occluded. However, shorter chains that cannot simultaneously reach both the tethering site and the catalytic site are nonproductively bound away from the catalytic center,[37] presumably along the exposed hydrophobic groove. With PvdQ, it is unlikely that the shorter chains are nonproductively bound but are rather just excluded from binding at the acyl-group binding site by the relatively polar entryway, illustrating by comparison two different ways in which ligands with shorter *n*-alkyl substituents can be disfavored.

The unexpected binding conformation for the short-chained *n*-alkylboronates is also notable in that it is unique for all structurally characterized PvdQ ligands. The product complexes and all of the inhibitors reported to date bind deep within the hydrophobic acyl-group binding site.[8−10,14] However, the adducts formed between C2- or C4-$B(OH)_2$ and S217 instead extend outward toward the headgroup binding site (Figures 4 and 5). This binding conformation may mimic the placement of the glutamine residue linking the myristic acid to the rest of the pyoverdine precursor substrate (Figure 1) and provides more information about how native substrates may bind. The fragment-sized[39] *n*-alkylboronic acid inhibitors C2- and C4-$B(OH)_2$ therefore represent promising lead compounds with excellent ligand efficiency[40] values (0.7 and 0.6 kcal/mol/non-H atom, respectively) suitable for the future development of inhibitors that specifically target the headgroup binding site, rather than the less-selective hydrophobic acyl-group binding site, with the goal of designing more selective H-bonding interactions with PvdQ.

CONCLUSION

The ligand binding selectivity of PvdQ is of interest both for engineering improved variants of the enzyme as a quorum-quenching catalyst and for designing small molecule inhibitors to block biosynthesis of the siderophore pyoverdine. Herein, a series of *n*-alkylboronic acids were used to investigate the dependence of *n*-alkyl chain length on binding affinity and orientation. Inhibitors with shorter *n*-alkyl substituents are found to be excluded from the acyl-group binding site by a polar entryway, but those with longer substituents can access a portion of this site highly optimized for hydrophobic binding, with affinity increasing −1.0 kcal/mol/CH_2 as the alkyl chain enters the site, until reaching the steric limit of the cavity, which correspond to a myristic acid substituent. These findings suggest a model for substrate discrimination to explain how PvdQ selectively processes substrates with longer *n*-acyl substituents, yet excludes structurally similar, but smaller, substrates that are encountered *in vivo*, such as the *N*-butanoyl-L-homoserine lactone quorum-sensing signal, to avoid perturbing these signaling pathways. The unexpected binding conformation of shorter *n*-alkylboronic acid inhibitors also provides the first example of an inhibitor accessing the headgroup binding site, which has more H-bonding partners available for the design of selective inhibitors.

ASSOCIATED CONTENT

Accession Codes

Coordinates and structure factors have been submitted to the Protein Data Bank with accession codes as follows: PvdQ:C2-$B(OH)_2$ (4WKS), PvdQ:C4-$B(OH)_2$ (4WKT), PvdQ:C6-$B(OH)_2$ (4WKU), PvdQ:C8-$B(OH)_2$ (4WKV).

AUTHOR INFORMATION

Corresponding Authors

*(W.F., for correspondence regarding enzymology) Mailing address: University of Texas at Austin, 107 W. Dean Keeton St., Stop C0850, BME 6.202D, Austin, TX 78712-1081. Tel: 512-232-4000. Fax: 512-232-2606. E-mail: walt.fast@austin.utexas.edu.

*(D.L., for correspondence regarding X-ray structure determinations) Tel: 773-508-3093. E-mail: dliu@luc.edu.

Author Contributions

#K.D.C. (enzymology) and R.W. (structure) share first authorship.

Funding

This work was supported in part by the National Science Foundation under Grant Number CHE-1308672 (to W.F. and D.L.), by the Robert A. Welch Foundation (F-1572 to W.F.), and by Loyola University Chicago (to D.L.).

Notes

The authors declare no competing financial interest.

ACKNOWLEDGMENTS

We thank the GM/CA-CAT staff, especially Dr. Ruslan Sanishvili, for help with data collection. GM/CA@APS has been funded in whole or in part with Federal funds from the National Cancer Institute (ACB-12002) and the National Institute of General Medical Sciences (AGM-12006). This research used resources of the Advanced Photon Source, a U.S. Department of Energy (DOE) Office of Science User Facility operated for the DOE Office of Science by Argonne National Laboratory under Contract No. DE-AC02-06CH11357.

REFERENCES

(1) Foley, T. L., and Simeonov, A. (2012) Targeting iron assimilation to develop new antibacterials. *Expert Opin. Drug Discovery 7*, 831−847.

(2) Amara, N., Krom, B. P., Kaufmann, G. F., and Meijler, M. M. (2011) Macromolecular inhibition of quorum sensing: enzymes, antibodies, and beyond. *Chem. Rev. 111*, 195−208.

(3) Oinonen, C., and Rouvinen, J. (2000) Structural comparison of Ntn-hydrolases. *Protein Sci. 9*, 2329−2337.

(4) Huang, J. J., Han, J. I., Zhang, L. H., and Leadbetter, J. R. (2003) Utilization of acyl-homoserine lactone quorum signals for growth by a soil pseudomonad and *Pseudomonas aeruginosa* PAO1. *Appl. Environ. Microbiol. 69*, 5941−5949.

(5) Lamont, I. L., and Martin, L. W. (2003) Identification and characterization of novel pyoverdine synthesis genes in *Pseudomonas aeruginosa*. *Microbiology 149*, 833−842.

(6) Yeterian, E., Martin, L. W., Guillon, L., Journet, L., Lamont, I. L., and Schalk, I. J. (2010) Synthesis of the siderophore pyoverdine in *Pseudomonas aeruginosa* involves a periplasmic maturation. *Amino Acids 38*, 1447−1459.

(7) Hannauer, M., Schafer, M., Hoegy, F., Gizzi, P., Wehrung, P., Mislin, G. L., Budzikiewicz, H., and Schalk, I. J. (2012) Biosynthesis of the pyoverdine siderophore of *Pseudomonas aeruginosa* involves precursors with a myristic or a myristoleic acid chain. *FEBS Lett. 586*, 96−101.

(8) Bokhove, M., Nadal Jimenez, P., Quax, W. J., and Dijkstra, B. W. (2010) The quorum-quenching *N*-acyl homoserine lactone acylase PvdQ is an Ntn-hydrolase with an unusual substrate-binding pocket. *Proc. Natl. Acad. Sci. U. S. A. 107*, 686−691.

(9) Drake, E. J., and Gulick, A. M. (2011) Structural characterization and high-throughput screening of inhibitors of PvdQ, an NTN hydrolase involved in pyoverdine synthesis. *ACS Chem. Biol. 6*, 1277−1286.

(10) Clevenger, K. D., Wu, R., Er, J. A., Liu, D., and Fast, W. (2013) Rational design of a transition state analogue with picomolar affinity

for *Pseudomonas aeruginosa* PvdQ, a siderophore biosynthetic enzyme. *ACS Chem. Biol. 8*, 2192−2200.
(11) Nadal Jimenez, P., Koch, G., Papaioannou, E., Wahjudi, M., Krzeslak, J., Coenye, T., Cool, R. H., and Quax, W. J. (2010) Role of PvdQ in *Pseudomonas aeruginosa* virulence under iron-limiting conditions. *Microbiology 156*, 49−59.
(12) Meyer, J. M., Neely, A., Stintzi, A., Georges, C., and Holder, I. A. (1996) Pyoverdin is essential for virulence of *Pseudomonas aeruginosa*. *Infect. Immun. 64*, 518−523.
(13) Lehoux, D. E., Sanschagrin, F., and Levesque, R. C. (2000) Genomics of the 35-kb *pvd* locus and analysis of novel *pvd*IJK genes implicated in pyoverdine biosynthesis in *Pseudomonas aeruginosa*. *FEMS Microbiol Lett. 190*, 141−146.
(14) Wurst, J. M., Drake, E. J., Theriault, J. R., Jewett, I. T., VerPlank, L., Perez, J. R., Dandapani, S., Palmer, M., Moskowitz, S. M., Schreiber, S. L., Munoz, B., and Gulick, A. M. (2014) Identification of Inhibitors of PvdQ, an Enzyme Involved in the Synthesis of the Siderophore Pyoverdine. *ACS Chem. Biol. 9*, 1536−1544.
(15) Papaioannou, E., Wahjudi, M., Nadal-Jimenez, P., Koch, G., Setroikromo, R., and Quax, W. J. (2009) Quorum-quenching acylase reduces the virulence of *Pseudomonas aeruginosa* in a *Caenorhabditis elegans* infection model. *Antimicrob. Agents Chemother. 53*, 4891−4897.
(16) Wahjudi, M., Murugappan, S., van Merkerk, R., Eissens, A. C., Visser, M. R., Hinrichs, W. L., and Quax, W. J. (2013) Development of a dry, stable and inhalable acyl-homoserine-lactone-acylase powder formulation for the treatment of pulmonary *Pseudomonas aeruginosa* infections. *Eur. J. Pharm. Sci. 48*, 637−643.
(17) Koch, G., Nadal-Jimenez, P., Reis, C. R., Muntendam, R., Bokhove, M., Melillo, E., Dijkstra, B. W., Cool, R. H., and Quax, W. J. (2014) Reducing virulence of the human pathogen *Burkholderia* by altering the substrate specificity of the quorum-quenching acylase PvdQ. *Proc. Natl. Acad. Sci. U. S. A. 111*, 1568−1573.
(18) Bissantz, C., Kuhn, B., and Stahl, M. (2010) A medicinal chemist's guide to molecular interactions. *J. Med. Chem. 53*, 5061−5084.
(19) Freire, E. (2008) Do enthalpy and entropy distinguish first in class from best in class? *Drug Discovery Today 13*, 869−874.
(20) Davis, B. M., Richens, J. L., and O'Shea, P. (2011) Label-free critical micelle concentration determination of bacterial quorum sensing molecules. *Biophys. J. 101*, 245−254.
(21) Smith, R., and Tanford, C. (1972) The critical micelle concentration of L-α- dipalmitoylphosphatidylcholine in water and water-methanol solutions. *J. Mol. Biol. 67*, 75−83.
(22) Copeland, R. A. (2005) *Evaluation of Enzyme Inhibitors in Drug Discovery*, pp 117−121, Wiley-Interscience, Hoboken, NJ.
(23) Cheng, Y., and Prusoff, W. H. (1973) Relationship between the inhibition constant (K_1) and the concentration of inhibitor which causes 50% inhibition (I_{50}) of an enzymatic reaction. *Biochem. Pharmacol. 22*, 3099−3108.
(24) Otwinowski, Z., and Minor, W. (1997) Processing of X-ray Diffraction Data Collected in Oscillation Mode. *Methods Enzymol. 276*, 307−326.
(25) Winn, M. D., Ballard, C. C., Cowtan, K. D., Dodson, E. J., Emsley, P., Evans, P. R., Keegan, R. M., Krissinel, E. B., Leslie, A. G., McCoy, A., McNicholas, S. J., Murshudov, G. N., Pannu, N. S., Potterton, E. A., Powell, H. R., Read, R. J., Vagin, A., and Wilson, K. S. (2011) Overview of the CCP4 suite and current developments. *Acta Crystallogr. D Biol. Crystallogr. 67*, 235−242.
(26) Emsley, P., Lohkamp, B., Scott, W. G., and Cowtan, K. (2010) Features and development of *Coot*. *Acta Crystallogr. D Biol. Crystallogr. 66*, 486−501.
(27) Lebedev, A. A., Young, P., Isupov, M. N., Moroz, O. V., Vagin, A. A., and Murshudov, G. N. (2012) JLigand: a graphical tool for the CCP4 template-restraint library. *Acta Crystallogr. D Biol. Crystallogr. 68*, 431−440.
(28) Adams, P. D., Grosse-Kunstleve, R. W., Hung, L. W., Ioerger, T. R., McCoy, A. J., Moriarty, N. W., Read, R. J., Sacchettini, J. C., Sauter, N. K., and Terwilliger, T. C. (2002) PHENIX: building new software for automated crystallographic structure determination. *Acta Crystallogr. D Biol. Crystallogr. 58*, 1948−1954.
(29) Pettersen, E. F., Goddard, T. D., Huang, C. C., Couch, G. S., Greenblatt, D. M., Meng, E. C., and Ferrin, T. E. (2004) UCSF Chimera–a visualization system for exploratory research and analysis. *J. Comput. Chem. 25*, 1605−1612.
(30) Hansch, C., and Coats, E. (1970) Alpha-chymotrypsin: a case study of substituent constants and regression analysis in enzymic structure–activity relationships. *J. Pharm. Sci. 59*, 731−743.
(31) Fersht, A. (1999) *Structure and Mechanism in Protein Science*, p 336, W.H. Freeman and Company, New York.
(32) Pace, C. N. (1992) Contribution of the hydrophobic effect to globular protein stability. *J. Mol. Biol. 226*, 29−35.
(33) Kuntz, I. D., Chen, K., Sharp, K. A., and Kollman, P. A. (1999) The maximal affinity of ligands. *Proc. Natl. Acad. Sci. U. S. A. 96*, 9997−10002.
(34) Leung, C. S., Leung, S. S., Tirado-Rives, J., and Jorgensen, W. L. (2012) Methyl effects on protein-ligand binding. *J. Med. Chem. 55*, 4489−4500.
(35) Powell, P. J., Lau, S. M., Killian, D., and Thorpe, C. (1987) Interaction of acyl coenzyme A substrates and analogues with pig kidney medium-chain acyl-coA dehydrogenase. *Biochemistry 26*, 3704−3710.
(36) Hall, D. G. (2005) Structure, Properties, and Prepartion of Boronic Acid Derivatives. Overview of Their Reactions and Applications, In *Boronic Acids* (Hall, D. G., Ed.), pp 8−12, Wiley-VCH, Weinheim, Germany.
(37) Chakravarty, B., Gu, Z., Chirala, S. S., Wakil, S. J., and Quiocho, F. A. (2004) Human fatty acid synthase: structure and substrate selectivity of the thioesterase domain. *Proc. Natl. Acad. Sci. U. S. A. 101*, 15567−15572.
(38) Zhang, W., Chakravarty, B., Zheng, F., Gu, Z., Wu, H., Mao, J., Wakil, S. J., and Quiocho, F. A. (2011) Crystal structure of FAS thioesterase domain with polyunsaturated fatty acyl adduct and inhibition by dihomo-gamma-linolenic acid. *Proc. Natl. Acad. Sci. U. S. A. 108*, 15757−15762.
(39) Congreve, M., Carr, R., Murray, C., and Jhoti, H. (2003) A 'rule of three' for fragment-based lead discovery? *Drug Discovery Today 8*, 876−877.
(40) Hopkins, A. L., Groom, C. R., and Alex, A. (2004) Ligand efficiency: a useful metric for lead selection. *Drug Discovery Today 9*, 430−431.